JACS Au
AN OPEN ACCESS JOURNAL OF THE AMERICAN CHEMICAL SOCIETY

pubs.acs.org/jacsau

Article

Manipulating Single-Walled Carbon Nanotube Arrays for Flexible Photothermoelectric Devices

Heng Wang, Rui Wang, Cheng Chen, Zhan Zhou, and Jian-Wei Liu*

Cite This: JACS Au 2022, 2, 2269−2276

Read Online

ACCESS | Metrics & More | Article Recommendations | Supporting Information

ABSTRACT: Flexible photothermoelectric (PTE) devices possess great application prospects in the field of light energy and thermoelectric energy harvesting which are some of the cornerstones of modern green renewable energy power generation. However, the low efficiency of PTE materials and lack of suitable manufacturing processes remain an impediment to restrict its rapid development. Here, we designed a flexible PTE device by printing a highly integrated single-walled carbon nanotubes (SWCNTs) array at intervals that were surface-functionalized with poly(acrylic acid) and poly(ethylene imine) as p−n heterofilms. After the introduction of a mask to give a selective light illumination and taking advantage of the photothermal effect of SWCNTs, a remarkable temperature gradient along the printed SWCNTs and a considerable power density of 1.3 $\mu W/cm^2$ can be achieved. Meanwhile, both experimental data and COMSOL theoretical simulations were adopted to optimize the performance of our device, showing new opportunities for new generation flexible PTE devices.

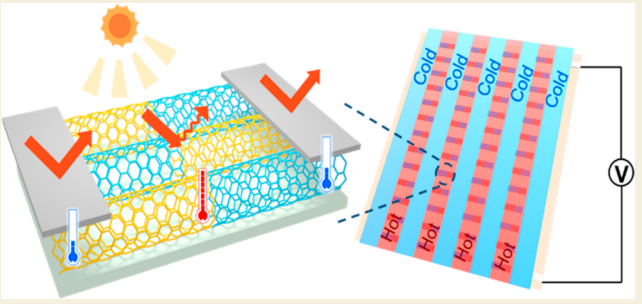

KEYWORDS: *thermoelectric materials, extrusion printing, single-walled carbon nanotubes, photothermoelectric devices, nanotube arrays*

INTRODUCTION

Light energy and thermoelectric energy harvesting are some of the cornerstones of modern green renewable energy power generation.[1−9] Unfortunately, conventional inorganic semiconductor thermoelectric generators have the disadvantages of being expensive, rigid, and prone to failure.[10−12] Converting environmental energy into electrical energy through flexible, wearable, stretchable, and expandable devices has always been one of the research hotspots of modern energy science.[13−17] In recent years, many new semiconductor materials have been developed to achieve this goal, and combining these materials with modern manufacturing technologies can also pave the way for cost-effective and scalable thermoelectric power generation. Printing strategies were frequently used to manufacture thermoelectric materials for scalable and flexible photothermoelectric (PTE) devices, such as screen printing, inkjet printing, and extrusion printing which have many advantages because of their ability to directly convert nanomaterial inks to the micrometer/millimeter scale with greatly reduced cost.[18−23] Bismuth telluride was often used as a thermoelectric material for printable inorganic ink. Although having a certain degree of flexibility, it still requires a sintering process up to 500 °C to achieve high performance, which limits the choice of flexible substrates.[24−26] The conductive polymer is also a printable thermoelectric material that was widely studied.[27−31] However, due to the lack of an n-type material that is insensitive to humidity under normal environmental conditions, conductive polymers are limited in practical applications. As another option, carbon nanotubes (CNTs) have good mechanical properties, such as strength and flexibility, and therefore have great potential in printed thermoelectric materials.[32−35] Mehmood et al. designed a bracelet-type thermoelectric structure in which the carbon nanotube ink was printed in the in-plane direction of the flexible tube, and the device was operated in the out-of-plane direction of the heat source.[34] To print carbon nanotube inks on curved surfaces, basic research has been conducted on the viscosity, dispersibility, and thermoelectric properties of carbon nanotube inks.[36] However, the output power of this research is low, it is difficult to apply to practice, the printing process is more complicated due to the device structure, and it is difficult to mass produce.

Herein, we used low-cost single-walled carbon nanotubes (SWCNTs) as inks to highly integrate SWCNT arrays at intervals for PTE devices which can first absorb light energy into heat energy and then convert it into electrical energy. First, SWCNTs were surface-functionalized with poly(acrylic acid) and poly(ethylene imine) as p−n thermoelectric

Received: March 24, 2022
Revised: August 29, 2022
Accepted: August 29, 2022
Published: September 8, 2022

https://doi.org/10.1021/jacsau.2c00189
JACS Au 2022, 2, 2269−2276

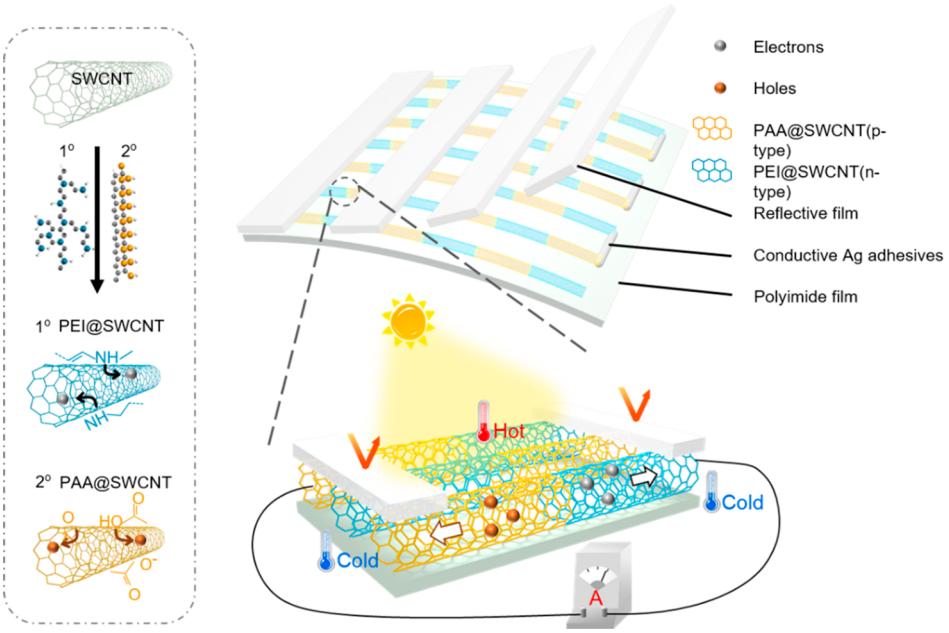

Figure 1. Schematic illustration of the photothermoelectric device printed with SWCNT inks.

materials. A silver reflective mask was introduced to achieve a considerable temperature difference under light radiation, and the maximum power density of our device can reach 1.3 μW/cm^2. COMSOL theoretical simulation was adopted to optimize the performance of our device. Finally, a new type of flexible photothermoelectric device structure was designed via a simple extrusion printing method and can be prepared continuously to achieve large-scale printing of highly integrated flexible photothermoelectric devices.

EXPERIMENTAL SECTION

Materials

Polyacrylic acid (PAA) (MW-2000) and poly(ethylenimine) (PEI) (MW-1000) were purchased from Aldrich. SWCNTs and surfactants were purchased from Best Materials.

Ink Preparation

The SWCNT ink was prepared by adding SWCNTs and surfactants in water and then fully dispersing them through an ultrasonic cell crusher (JY98-IIN, Xinzhi Biotech Co., Ltd., Ningbo, China) for 2 h. The ultrasonic power was 300 W, and the working time of the ultrasonic treatment was 2 s while the interval was 2 s. The ink was kept in the ice water bath to prevent overheating. To prepare n- and p-doping inks, PEI and PAA were added into the homogeneously distributed SWCNT ink with a concentration of 0.5 and 100 mg mL^{-1}, respectively. The concentration of the final doped SWCNT solutions was fixed at 5 mg mL^{-1}, and the mixtures were stirred for 12 h to obtain uniformly dispersed n- and p-type SWCNT inks.

Device Fabrication

We used a pneumatic extrusion type flexible electronics printer (MP1100, Prtronic, Shanghai, China) to perform device printing, which included programmable control of temperature and pressure. The n-type and p-type SWCNT inks were placed in 5 mL syringe barrels. The syringe had a nozzle with an inner diameter of 750 μm. The n-type SWCNT ink was printed on a polyimide film first. And then, the n-type SWCNT ink was printed on the same polyimide film. The printed pattern was designed by the drawing software that came with the flexible electronics printer. The printing pressure of n- and p-type inks were 12 and 10 KPa, respectively. The temperature of the printer platen that holds the polyimide film was set to 50 °C during printing. To reduce resistance, the n- and p-type circuits were printed five times each. Next, the silver conductive paint (SPI supplies, USA: SPI#05002-AB) was printed as electrodes and wires connecting the n- and p-type circuits. Finally, the reflective silver film was cut to a specific size and pasted on the printed circuit at a certain interval.

Characterization

Scanning electron microscopy (SEM) images were obtained by using a field emission scanning electron microanalyzer (Zeiss Supra 40 scanning electron microscope at an acceleration voltage of 5 kV). Transmission electron microscopy (TEM) was performed on a H-7650 instrument (Hitachi, Japan) operated at an acceleration voltage of 100 kV. The Raman spectra were measured using a LabRAM HR instrument (HORIBA Jobin Yvon Inc.). The in-plane electrical conductivity of the n- and p-type SWCNT inks were measured by using an M-3 portable four-point probe test meter (Suzhou lattice electron Limited company, China). The Seebeck coefficients of the n- and p-type inks were acquired using the Seebeck coefficient measuring instrument (SBA 458, NETZSCH, German). The resistance and voltage were measured using a Keithley 7510 multimeter which was controlled by KickStart software on a computer. The thickness of the printed circuit was tested by using a surface profiler (KLA-Tencor, P17).

RESULTS AND DISCUSSION

Fabrication of the Photothermoelectric Device

To design a new type of flexible photothermoelectric device structure, we used two kinds of doped SWCNTs to construct a continuous p−n junction structure by integrated printing. At the same time, a local silver reflective layer was introduced to shield the light absorption under the reflective layer. In this way, the temperature of the exposed part of the carbon nanotube nodes increases due to light absorption, and the carbon nanotubes under the reflective layer have no temperature change. Therefore, we introduced a temperature gradient on the plane and converted the temperature gradient into electrical energy through the carbon nanotube p−n junction thermopile. This extrusion printing method is very simple and can be prepared continuously to achieve large-scale printing of highly integrated flexible photothermoelectric devices (Figure 1).

https://doi.org/10.1021/jacsau.2c00189
JACS Au 2022, 2, 2269−2276

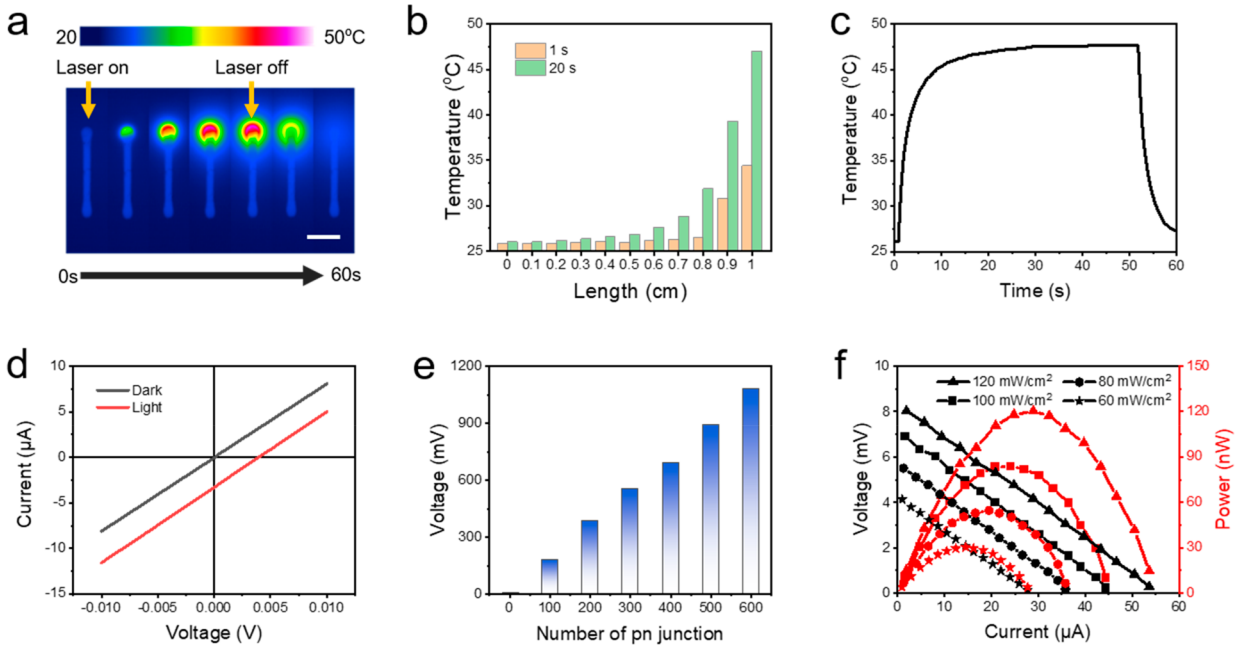

Figure 2. Performance of photothermoelectric devices. (a) Infrared thermal imaging of one end of the printed circuit irradiated with a laser. (b) Histogram of the temperature distribution of the printed circuit after being irradiated by the laser for 1 and 20 s. (c) Temperature change curve of laser irradiation point. (d) Volt−ampere characteristic curve and (e) relationship between the output voltage and the number of printed p−n junctions. (f) Power curve of the device under different light intensity.

Compared with other thermoelectric materials such as bismuth telluride, carbon nanotubes can achieve ideal thermoelectric performance without high temperature and high-pressure processing, so they are very suitable for printing thermoelectric devices on flexible substrates that are not resistant to high temperatures.[37−39] At the same time, the high absorbance of the single-walled carbon nanotube itself can make it absorb light energy and convert it into heat energy for power generation. In addition, it does not require expensive raw materials and complicated preparation processes and can be obtained at a lower cost, which greatly reduces the preparation process and cost of the device. Finally, due to the high conductivity of single-walled carbon nanotubes, the internal resistance of the device is reduced to a certain extent, and the output power is increased.

In the production of ink, we used the purchased SWCNTs (Figure S1) and a commercial surfactant to be dispersed in water. Because the single-walled carbon nanotubes are hydrophobic, the surfactants are needed to help with dispersion during the dispersion process. In addition, the ink used for extrusion printing needs a certain viscosity, so the concentration of single-walled carbon nanotubes in the ink needs to be relatively high to ensure the stability and integrity of the ink during extrusion printing and, at the same time, reduce the resistance of ink. During the dispersion process, we used an ultrasonic cell crusher to fully disperse the SWCNTs to prevent the needle from clogging during printing due to uneven dispersion of the carbon nanotubes.

To construct a p−n junction thermopile, we used organic small molecule doping to obtain p-type and n-type SWCNTs (Figure S2). We mainly used PAA and PEI small molecules for doping. To explore the effect of different doping concentrations on the Seebeck coefficient and conductivity of the ink, we added 0.1%, 0.5%, 5%, 10%, and 20% mass fraction of PAA and 5%, 10%, 25%, 50%, and 90% mass fraction of PEI to the dispersed SWCNTs ink. The results obtained are shown in Figure S3. When the PAA doped mass fraction is about 10%, the Seebeck coefficient of the p-type ink reaches the maximum (Figure S3a). When the PEI doping mass fraction is about 0.5%, the Seebeck coefficient of the n-type ink reaches the maximum value (Figure S3b), and the conductivity of the two inks does not change much under different doping concentrations.

After obtaining the ideal doping concentration, PAA and PEI were added to the dispersed ink, and p-type and n-type single-walled carbon nanotubes were obtained after long-term stirring. If the stirring time is insufficient, PAA and PEI are not sufficiently doped on the surface of the carbon nanotubes, and the Seebeck coefficient of the resulting ink will be lower. The PAA is an effective moisture absorbing material because it has many carboxylic acid groups, which makes it hydrophilic. The water and oxygen molecules are adsorbed on the surface of the SWCNTs, and this leads to p-doping, which has been reported in the previous literature.[33,40,41] And PEI is an excellent n-dopant because it has electron-donating amine groups. When PEI is wrapped on the SWCNT surface, the majority of carriers are changed from holes to electrons, which changes the SWCNTs from p- to n-type.[32,42,43] From the SEM image and TEM image of the ink (Figure S4), it can be seen that, after mixing and doping, the morphology of the single-walled carbon nanotubes does not change significantly, and they are still uniformly dispersed. This provided the foundation for the next printing process. Moreover, we made a comparison of normalized Raman spectra of doped and undoped SWCNTs that were excited with a 514 nm laser (Figure S5). After being doped with PAA and PEI, the ratio of the G band and D* band changed, because the degree of defect affects the D* band and G band.[44]

Considering that when the photothermoelectric device works under sunlight, the surface of the device will rise to a

https://doi.org/10.1021/jacsau.2c00189
JACS Au 2022, 2, 2269−2276

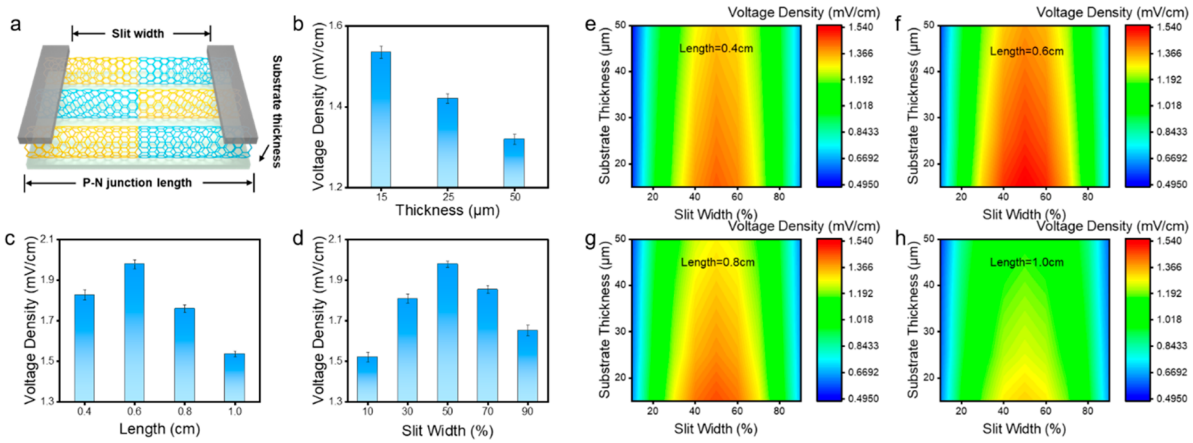

Figure 3. Adjustment of device performance. (a) Schematic diagram of three adjustment parameters. Test results for different sizes of (b) substrate thickness, (c) p−n junction length, and (d) slit width. The COMSOL simulation for different sizes of substrate thickness and slit width at different p−n junction lengths at (e) 0.4 cm, (f) 0.6 cm, (g) 0.8 cm, and (h) 1.0 cm.

higher temperature due to the absorption of light energy into heat energy by the single-walled carbon nanotubes. To verify that the performance of the device remains stable at different operating temperatures, we further measured the Seebeck coefficient of the two inks at 25, 35, 45, 55, 65, and 75 °C (Figure S6). As shown by the results, the Seebeck coefficient of two SWCNT inks does not change much in the operating temperature range of 25−75 °C.

For the selection of the flexible substrate material, we used a polyimide film as the flexible substrate. First, the polyimide film is an insulating material to ensure that the device will not be short-circuited. Second, because our device is running under sunlight. The maximum operating temperature can reach 70 °C, so we need a high-temperature resistant film. In addition, because the polyimide film we purchased is black, the black substrate can also absorb sunlight and heat up, so that the hot end of the device can reach a higher temperature which further improves the output power of the device. In summary, we purchased a commercial polyimide film as our flexible substrate. For the choice of reflective film, we magnetron sputtered a layer of silver film on the PET film, and its reflectivity remained above 95% in the wavelength range of 400−2500 nm (Figure S7).

To explore the endothermic and thermal conductivity of carbon nanotubes, we irradiated one end of a printed SWCNT line with a 365 nm laser and obtained the infrared thermal image as shown in Figure 2a. We can see that the heat transfer distance at the hot end is 2−4 mm (Figure 2b) and the temperature tends to be stable after about 20 s (Figure 2c). This helps us control the distance between the hot end and cold end to ensure that the distance is as short as possible to prevent heat from the hot end from diffusing to the cold end, and it also can reflect the response speed of the device. We also carried out thermal infrared imaging of the device, showing the temperature difference between the hot end and the cold end during the working process, and more intuitively showing the diffusion and distribution of temperature in the device and how the photothermal effect assists to generate the power (Figure S8). And after printing, the SWCNTs are densely intertwined (Figure S9).

To further verify that the power generation mechanism of the device is the photothermoelectric effect, we tested the volt−ampere characteristic curve of the carbon nanotube device (Figure 2d). It can be found that the volt−ampere characteristic curve shows a straight line regardless of light or light conditions, which shows that there is no barrier effect such as the p−n junction barrier. And the curve under the light environment deviates from the origin, which also shows that the internal electric potential is generated. This fully demonstrates that the generator principle of the carbon nanotube generator prepared in this experiment is the photothermoelectric effect.

We prepared a generator composed of three pairs of p−n junctions and used it for testing, and found that the device can output electrical signals stably under sunlight. Then we keep increasing the number of p−n junctions printed on the polyimide film and measured the output voltage (Figure 2e). It can be found that with the increase in the number of printed p−n junction pairs, the output voltage also increases, and the number of p−n junction pairs and the voltage have an obvious linear relationship, which also illustrates the performance stability of carbon nanotube printing. The picture of a large area printed device on a 13*13 cm polyimide film is shown in Figure S10, and the output power is as high as 64.6 μW. The schematic diagram of the device performance test is also provided in Figure S11. At the same time, we also measured the output power of the device (Figure 2f). It can be found that the output power of the device changes with the change of the external resistance, and its peak value is located near the position where the external resistance is equal to the internal resistance of the device. In a sunny day (80−100 mW/cm^2) environment, the total power can reach 85 nW, even in cloudy weather (40−60 mW/cm^2), the total power can reach 45 nW.

Optimization of Device Performance

During the printing and preparation process of the device, various printing parameters of the carbon nanotube ink will affect the device, such as the thickness of the ink, the length of the p−n junction, and the interval between two stripes (Figure 3a). In addition, the thickness of the flexible substrate and the width of the reflective film also affect the performance of the device. After determining the material selection, to obtain the optimal printing parameters and material parameters, after analysis, we made a series of adjustments to the three parameters, namely, the thickness of the polyimide film, the length of the single p−n junction, and the slit width. For our photothermoelectric devices, their performance is reflected in

https://doi.org/10.1021/jacsau.2c00189
JACS Au 2022, 2, 2269−2276

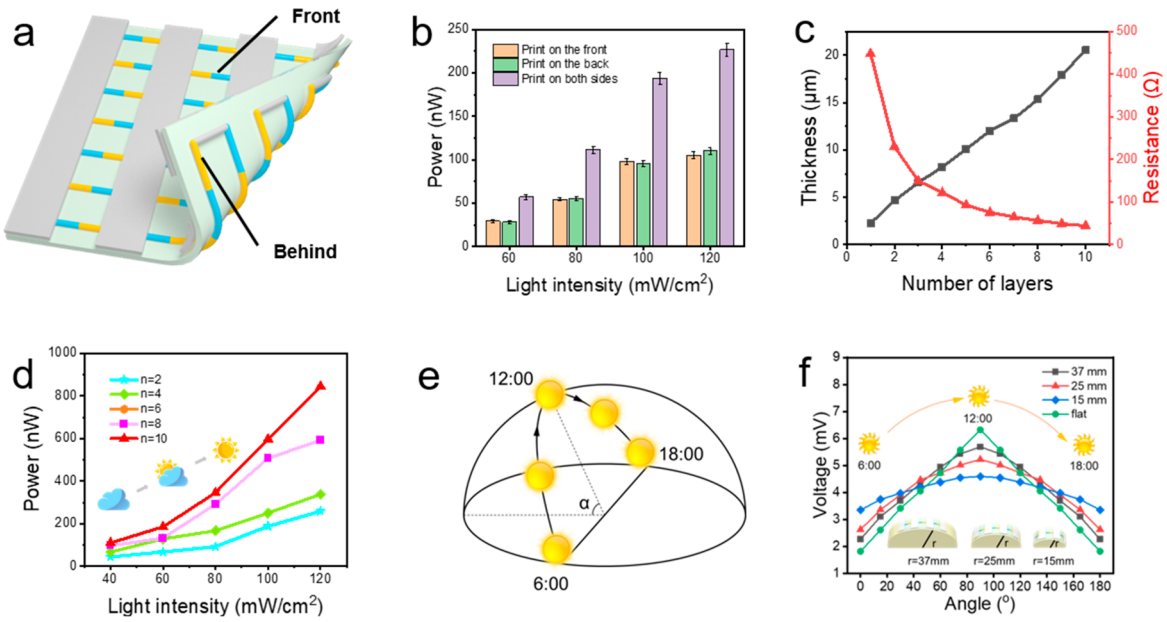

Figure 4. (a) Schematic diagram of a double-sided printed device and (b) its power test under different light intensity. (c) Thickness variation and resistance variation of printed SWCNTs with different numbers of layers from 1 to 10 layers. (d) Power of devices with different numbers of layers under different light intensities. (e) Schematic diagram of the change of the altitude angle of the sun during the day. (f) Under different illumination angles, the change curve of the output voltage of the device with different bending angles.

the output voltage density, that is, the voltage that can be provided per unit length.

First, to increase the output voltage, we need to increase the temperature difference between the cold and hot ends of the p−n junction in the device. For the hot end, that is, the part that receives sunlight, the polyimide substrate of different thicknesses absorbs heat differently. The amount of heat absorbed by the substrate will affect the maximum temperature that the hot end can eventually reach. In addition, the width of the slit will affect the area of the device that absorbs sunlight, which will affect the amount of heat absorbed by the hot end. Second, to increase the voltage density, the shorter the length of the p−n junction under a certain voltage, the higher the voltage density the device can output. However, considering that the SWCNTs have heat transfer, to realize that the temperature of the hot end is not transferred to the cold end, the length of a single p−n junction cannot be less than 2 mm. Therefore, to adjust the optimal parameters, we tested a series of data and obtained the data shown in Figure 3b−d. When the thickness of the polyimide film is 15 μm, the length of the single p−n junction is 0.6 cm, the slit width is 50% of the length of a pair of p−n junctions, and the output voltage per unit length reaches the maximum value. It can be seen that the optimal parameter conditions are consistent with the experimental results. Then we tested the power density of the optimized device and found it could reach 1.3 μW/cm^2 (Figure S12). We use total area of the thermoelectric leg (i.e., width × length × # of legs) to calculate the power density as previously reported.[45]

To ensure the accuracy of the control results, we used the COMSOL simulation software to simulate the output voltage per unit length of the device under different parameters and obtained the results as shown in Figure 3e−h.

Because printing has the advantages of high repeatability, high stability, fast printing speed, programmability, etc., to further improve the power generation performance of carbon nanotube photothermoelectric devices, series integration can be used to print as many p−n junctions per unit area as possible, which can increase the output power per unit area. To this end, the thickness of the polyimide film is very small and the temperature drop in the thickness direction of the film is zero, which indicates that the temperature on the back of the film is the same as that on the irradiated surface. We designed a double-sided printing structure (Figure 4a) to improve the number of p−n junctions. Due to the high accuracy of the printing method, the front circuit and the back circuit are basically at the same position, which ensures that the temperature distribution of the carbon nanotube network on the front and back is the same. In this way, we continue to use the double-sided printing method to continue to increase the degree of serial integration of the devices. Specifically, the same ink is printed on the front and back sides of the polyimide film at the same position, and the front and back circuits are connected in series. From Figure 4b, it can be determined that the output voltage and output power of the double-sided printing are doubled, which can be used to further increase the output voltage and output power and thus increase the output power of the carbon nanotube photothermoelectric generator.

Low internal resistance is also one of the necessary conditions for the photothermoelectric generator. To study the resistance change of the printed carbon nanotube film, we printed different layers of the carbon nanotube strip film. It can be found that, with the increase of the number of printing layers, the thickness of the film is continuously increasing (Figure 4c) and shows a linear relationship, which also fully illustrates the uniformity of carbon nanotube printing. The resistance and the number of layers show an inverse relationship, because as the number of layers increases, the cross-sectional area of the conductive channel increases, and the resistance decreases. Then we tested the power of devices with different numbers of layers under different light intensities (Figure 4d), and we found that the power of the device

https://doi.org/10.1021/jacsau.2c00189
JACS Au 2022, 2, 2269−2276

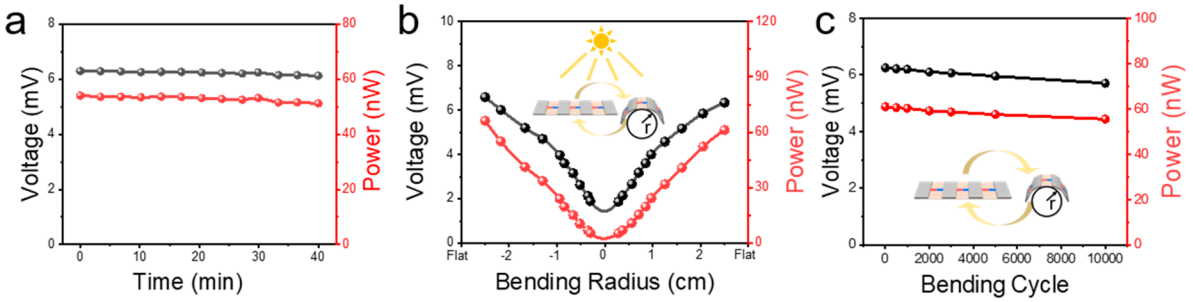

Figure 5. Fatigue test of the device. Variation curve of output voltage and output power with (a) working time, (b) bending radius, and (c) bending cycle.

increased with the number of printed layers and the light intensity. In a subsequent study, we adjusted the number of layers allowed to be five layers, which can avoid a too long printing time, greatly reduce the internal resistance of the device, and increase the output power.

Fatigue Test of the Device

Considering that, in practical applications, the position of the sun in a day is constantly changing (Figure 4e) and its elevation angle changes with time, we want to ensure that the device can generate electrical signals smoothly at any angle of sun irradiation. Thus, we need to design the shape of the device to try to make the sunlight intensity received by the device at any time consistent. To this end, we tested the changing trend of the output voltage with the light angle of the device composed of three pairs of p−n structures (total length is 4 cm) under different bending radii (Figure 4f). From the figure, we can see that the radius is 15 mm when the output voltage of the device is the most stable and the output voltage changes most obviously when the radius is 37 mm. Therefore, adjusting the bending radius when the device is working greatly improves the stability of the output power.

For a flexible device, its fatigue resistance is an important consideration. Therefore, we tested the fatigue resistance of the device composed of three pairs of p−n structures from three aspects (Figure 5). First, as the working time of the device gradually increases to 40 min, the output voltage is stable. Second, in the bending test, when the bending radius is gradually reduced, the voltage and output power both show a downward trend. This is because the sunlight received in the device is irradiated in parallel, whether in the test environment or the normal working environment. Therefore, when the device is bent, the area that receives light will decrease, so the output voltage and output power show a downward trend. When the bending test returns to a flat surface, the output voltage and output power of the device change within 5%, which can be seen in the device having excellent bending resistance. Finally, in the bending test, the output voltage and output power changed by 10% after 10 000 bending tests. Moreover, we also tested the output voltage of 10 devices to determine the repeatability of the achieved photothermoelectric performance (Figure S13). All devices used the same SWCNT inks and consisted of three pairs of p−n junctions, and during the test the light intensity was 100 mW/cm^2.

CONCLUSION

In summary, we present a scalable and low-cost manufacturing process to construct a new type of flexible photothermoelectric device structure. We used low-cost and easy-to-obtain SWCNTs to obtain n-type and p-type carbon nanotubes after doping and make them into printable inks. The ink was printed into a highly integrated array at intervals to design a device, and this device could first absorb light energy into heat energy and then convert it into electrical energy for use. Although this energy conversion seems like it may cause some energy loss, our photothermoelectric device is actually a kind of thermoelectronic device. The key point of our research is how we can use the waste heat in nature to generate useful electricity. So we use light as a source of waste heat. After testing, the output per unit length of the p−n junction could be obtained. Finally, a new type of flexible photothermoelectric device structure was designed via a simple extrusion printing method and can be prepared continuously to achieve large-scale printing of highly integrated flexible photothermoelectric devices. This research will pave the way for new opportunities for other nanothermoelectric materials.

ASSOCIATED CONTENT

Supporting Information

The Supporting Information is available free of charge at https://pubs.acs.org/doi/10.1021/jacsau.2c00189.

Materials; experimental details and supplementary results including reflectivity of the silver film, Seebeck coefficient and electrical conductivity of inks, power densities, device repeatability; SEM, TEM, and Raman spectra for all compounds; optical picture of inks and device; schematic diagram of the device; infrared image of the device (PDF)

AUTHOR INFORMATION

Corresponding Author

Jian-Wei Liu − *Division of Nanomaterials & Chemistry, Hefei National Research Center for Physical Sciences at the Microscale, Department of Chemistry, Institute of Biomimetic Materials & Chemistry, University of Science and Technology of China, Hefei 230026, China;* orcid.org/0000-0001-9237-1025; Email: jwliu13@ustc.edu.cn

Authors

Heng Wang − *Division of Nanomaterials & Chemistry, Hefei National Research Center for Physical Sciences at the Microscale, Department of Chemistry, Institute of Biomimetic Materials & Chemistry, University of Science and Technology of China, Hefei 230026, China*

Rui Wang − *Division of Nanomaterials & Chemistry, Hefei National Research Center for Physical Sciences at the Microscale, Department of Chemistry, Institute of Biomimetic*

https://doi.org/10.1021/jacsau.2c00189
JACS Au 2022, 2, 2269−2276

Materials & Chemistry, University of Science and Technology of China, Hefei 230026, China

Cheng Chen − *Division of Nanomaterials & Chemistry, Hefei National Research Center for Physical Sciences at the Microscale, Department of Chemistry, Institute of Biomimetic Materials & Chemistry, University of Science and Technology of China, Hefei 230026, China*

Zhan Zhou − *Division of Nanomaterials & Chemistry, Hefei National Research Center for Physical Sciences at the Microscale, Department of Chemistry, Institute of Biomimetic Materials & Chemistry, University of Science and Technology of China, Hefei 230026, China*

Complete contact information is available at: https://pubs.acs.org/10.1021/jacsau.2c00189

Author Contributions

H.W. and J.-W.L. planned and performed the experiments, collected and analyzed the data, and wrote the paper. C.C. and Z.Z. helped with the synthesis of the materials and collected the data. J.-W.L. and R.W. analyzed the data and cowrote the manuscript. All authors analyzed and discussed the results. Competing financial interests.

Notes

The authors declare no competing financial interest.

■ ACKNOWLEDGMENTS

The authors acknowledge financial support from the National Natural Science Foundation of China (Grants 21922204, 22175164) and the Joint Funds from Hefei National Synchrotron Radiation Laboratory (UN2018LHJJ). This work was partially carried out at the USTC Center for Micro and Nanoscale Research and Fabrication.

■ REFERENCES

(1) Hong, S.; Gu, Y.; Seo, J. K.; Wang, J.; Liu, P.; Meng, Y. S.; Xu, S.; Chen, R. K. Wearable thermoelectrics for personalized thermoregulation. *Sci. Adv.* **2019**, *5* (5), 11.

(2) Yang, Y.; Wang, J. L.; Liu, L.; Wang, Z. H.; Liu, J. W.; Yu, S. H. A room-temperature environmentally friendly solution process to assemble silver nanowire architectures for flexible transparent electrodes. *Nanoscale* **2017**, *9* (1), 52−55.

(3) Liu, J. W.; Xu, J. E.; Ni, Y.; Fan, F. J.; Zhang, C. L.; Yu, S. H. A Family of Carbon-Based Nanocomposite Tubular Structures Created by in Situ Electron Beam Irradiation. *ACS Nano* **2012**, *6* (5), 4500−4507.

(4) Shi, X. L.; Zou, J.; Chen, Z. G. Advanced Thermoelectric Design: From Materials and Structures to Devices. *Chem. Rev.* **2020**, *120* (15), 7399−7515.

(5) Khan, S.; Kim, J.; Acharya, S.; Kim, W. Review on the operation of wearable sensors through body heat harvesting based on thermoelectric devices. *Appl. Phys. Lett.* **2021**, *118* (20), 200501.

(6) Shi, Q. F.; He, T. Y. Y.; Lee, C. More than energy harvesting - Combining triboelectric nanogenerator and flexible electronics technology for enabling novel micro-/nano-systems. *Nano Energy* **2019**, *57*, 851−871.

(7) Shepelin, N. A.; Glushenkov, A. M.; Lussini, V. C.; Fox, P. J.; Dicinoski, G. W.; Shapter, J. G.; Ellis, A. V. New developments in composites, copolymer technologies and processing techniques for flexible fluoropolymer piezoelectric generators for efficient energy harvesting. *Energy Environ. Sci.* **2019**, *12* (4), 1143−1176.

(8) Shrivastava, S.; Trung, T. Q.; Lee, N. E. Recent progress, challenges, and prospects of fully integrated mobile and wearable point-of-care testing systems for self-testing. *Chem. Soc. Rev.* **2020**, *49* (6), 1812−1866.

(9) Xu, C.; Song, Y.; Han, M. D.; Zhang, H. X. Portable and wearable self-powered systems based on emerging energy harvesting technology. *Microsyst. Nanoeng.* **2021**, *7* (1), 14.

(10) Zhou, M.; Al-Furjan, M. S. H.; Zou, J.; Liu, W. T. A review on heat and mechanical energy harvesting from human - Principles, prototypes and perspectives. *Renewable Sustainable Energy Rev.* **2018**, *82* (3), 3582−3609.

(11) Zhang, D.; Wang, Y. H.; Yang, Y. Design, Performance, and Application of Thermoelectric Nanogenerators. *Small* **2019**, *15* (32), 1805241.

(12) Yu, H.; Li, N.; Zhao, N. How Far Are We from Achieving Self-Powered Flexible Health Monitoring Systems: An Energy Perspective. *Adv. Energy Mater.* **2021**, *11* (9), 2002646.

(13) Suarez, F.; Nozariasbmarz, A.; Vashaee, D.; Ozturk, M. C. Designing thermoelectric generators for self-powered wearable electronics. *Energy Environ. Sci.* **2016**, *9* (6), 2099−2113.

(14) Wu, H.; Huang, Y. A.; Xu, F.; Duan, Y. Q.; Yin, Z. P. Energy Harvesters for Wearable and Stretchable Electronics: From Flexibility to Stretchability. *Adv. Mater.* **2016**, *28* (45), 9881−9919.

(15) Thielen, M.; Sigrist, L.; Magno, M.; Hierold, C.; Benini, L. Human body heat for powering wearable devices: From thermal energy to application. *Energy Convers. Manage.* **2017**, *131*, 44−54.

(16) Wang, L. M.; Zhang, Z. M.; Liu, Y. C.; Wang, B. R.; Fang, L.; Qiu, J. J.; Zhang, K.; Wang, S. R. Exceptional thermoelectric properties of flexible organic-inorganic hybrids with monodispersed and periodic nanophase. *Nat. Commun.* **2018**, *9*, 3817.

(17) Jin, Q.; Jiang, S.; Zhao, Y.; Wang, D.; Qiu, J. H.; Tang, D. M.; Tan, J.; Sun, D. M.; Hou, P. X.; Chen, X. Q.; et al. Flexible layer-structured Bi2Te3 thermoelectric on a carbon nanotube scaffold. *Nat. Mater.* **2019**, *18* (1), 62−68.

(18) Chen, B. L.; Kruse, M.; Xu, B.; Tutika, R.; Zheng, W.; Bartlett, M. D.; Wu, Y.; Claussen, J. C. Flexible thermoelectric generators with inkjet-printed bismuth telluride nanowires and liquid metal contacts. *Nanoscale* **2019**, *11* (12), 5222−5230.

(19) Feng, J. J.; Zhu, W.; Deng, Y.; Song, Q. S.; Zhang, Q. Q. Enhanced Antioxidation and Thermoelectric Properties of the Flexible Screen-Printed Bi2Te3 Films through Interface Modification. *ACS Appl. Energy Mater.* **2019**, *2* (4), 2828−2836.

(20) Hajiesmaili, E.; Khare, E.; Chortos, A.; Lewis, J.; Clarke, D. R. Voltage-controlled morphing of dielectric elastomer circular sheets into conical surfaces. *Extreme Mech. Lett.* **2019**, *30*, 100504.

(21) Jo, S.; Choo, S.; Kim, F.; Heo, S. H.; Son, J. S. Ink Processing for Thermoelectric Materials and Power-Generating Devices. *Adv. Mater.* **2019**, *31* (20), 1804930.

(22) Davidson, E. C.; Kotikian, A.; Li, S. C.; Aizenberg, J.; Lewis, J. A. 3D Printable and Reconfigurable Liquid Crystal Elastomers with Light-Induced Shape Memory via Dynamic Bond Exchange. *Adv. Mater.* **2020**, *32* (1), 1905682.

(23) Feng, J. Z.; Su, B. L.; Xia, H. S.; Zhao, S. Y.; Gao, C.; Wang, L. K.; Ogbeide, O.; Feng, J.; Hasan, T. Printed aerogels: chemistry, processing, and applications. *Chem. Soc. Rev.* **2021**, *50* (6), 3842−3888.

(24) Bae, E. J.; Kang, Y. H.; Jang, K. S.; Lee, C.; Cho, S. Y. Solution synthesis of telluride-based nano-barbell structures coated with PEDOT:PSS for spray-printed thermoelectric generators. *Nanoscale* **2016**, *8* (21), 10885−10890.

(25) Chen, B. L.; Das, S. R.; Zheng, W.; Zhu, B. W.; Xu, B.; Hong, S.; Sun, C. H.; Wang, X. W.; Wu, Y.; Claussen, J. C. Inkjet Printing of Single-Crystalline Bi2Te3 Thermoelectric Nanowire Networks. *Adv. Electron. Mater.* **2017**, *3* (4), 1600524.

(26) Kim, F.; Kwon, B.; Eom, Y.; Lee, J. E.; Park, S.; Jo, S.; Park, S. H.; Kim, B. S.; Im, H. J.; Lee, M. H.; et al. 3D printing of shape-conformable thermoelectric materials using all-inorganic Bi2Te3-based inks. *Nat. Energy* **2018**, *3* (4), 301−309.

(27) Soltman, D.; Subramanian, V. Inkjet-printed line morphologies and temperature control of the coffee ring effect. *Langmuir* **2008**, *24* (5), 2224−2231.

(28) Cho, C.; Wallace, K. L.; Tzeng, P.; Hsu, J. H.; Yu, C.; Grunlan, J. C. Outstanding Low Temperature Thermoelectric Power Factor

from Completely Organic Thin Films Enabled by Multidimensional Conjugated Nanomaterials. *Adv. Energy Mater.* **2016**, *6* (7), 1502168.
(29) Zhang, J. C.; Zhong, L. B.; Sun, Y. H.; Li, A. R.; Huang, J.; Meng, F. B.; Chandran, B. K.; Li, S. Z.; Jiang, L.; Chen, X. D. Enhanced Photoresponse of Conductive Polymer Nanowires Embedded with Au Nanoparticles. *Adv. Mater.* **2016**, *28* (15), 2978−2982.
(30) Huang, Z. D.; Su, M.; Yang, Q.; Li, Z.; Chen, S. R.; Li, Y. F.; Zhou, X.; Li, F. Y.; Song, Y. L. A general patterning approach by manipulating the evolution of two-dimensional liquid foams. *Nat. Commun.* **2017**, *8*, 14110.
(31) Li, D. D.; Lai, W. Y.; Zhang, Y. Z.; Huang, W. Printable Transparent Conductive Films for Flexible Electronics. *Adv. Mater.* **2018**, *30* (10), 1704738.
(32) Zhou, W. B.; Fan, Q. X.; Zhang, Q.; Cai, L.; Li, K. W.; Gu, X. G.; Yang, F.; Zhang, N.; Wang, Y. C.; Liu, H. P.; et al. High-performance and compact-designed flexible thermoelectric modules enabled by a reticulate carbon nanotube architecture. *Nat. Commun.* **2017**, *8*, 14886.
(33) Park, K. T.; Choi, J.; Lee, B.; Ko, Y.; Jo, K.; Lee, Y. M.; Lim, J. A.; Park, C. R.; Kim, H. High-performance thermoelectric bracelet based on carbon nanotube ink printed directly onto a flexible cable. *J. Mater. Chem. A* **2018**, *6* (40), 19727−19734.
(34) Mehmood, T.; Kim, J. H.; Lee, J.; Dizhur, S.; Hirst, E. S.; Ill, R. M. O.; Sayyad, M. H.; Munawar, M. A.; Xu, J. A flexible, printable, thin-film thermoelectric generator based on reduced graphene oxide-carbon nanotubes composites. *J. Mater. Sci.* **2020**, *55* (24), 10572−10581.
(35) Tzounis, L.; Petousis, M.; Grammatikos, S.; Vidakis, N. 3D Printed Thermoelectric Polyurethane/Multiwalled Carbon Nanotube Nanocomposites: A Novel Approach towards the Fabrication of Flexible and Stretchable Organic Thermoelectrics. *Materials* **2020**, *13* (12), 2879.
(36) Stuwe, D.; Mager, D.; Biro, D.; Korvink, J. G. Inkjet Technology for Crystalline Silicon Photovoltaics. *Adv. Mater.* **2015**, *27* (4), 599−626.
(37) Duong, H. M.; Yamamoto, N.; Bui, K.; Papavassiliou, D. V.; Maruyama, S.; Wardle, B. L. Morphology Effects on Nonisotropic Thermal Conduction of Aligned Single-Walled and Multi-Walled Carbon Nanotubes in Polymer Nanocomposites. *J. Phys. Chem. C* **2010**, *114* (19), 8851−8860.
(38) Hecht, D. S.; Hu, L. B.; Irvin, G. Emerging Transparent Electrodes Based on Thin Films of Carbon Nanotubes, Graphene, and Metallic Nanostructures. *Adv. Mater.* **2011**, *23* (13), 1482−1513.
(39) Marconnet, A. M.; Yamamoto, N.; Panzer, M. A.; Wardle, B. L.; Goodson, K. E. Thermal Conduction in Aligned Carbon Nanotube-Polymer Nanocomposites with High Packing Density. *ACS Nano* **2011**, *5* (6), 4818−4825.
(40) Yasunishi, T.; Kishimoto, S.; Ohno, Y. Effect of ambient air on n-type carbon nanotube thin-film transistors chemically doped with poly(ethylene imine). *Jpn. J. Appl. Phys.* **2014**, *53*, 05FD01.
(41) Hayashi, D.; Ueda, T.; Nakai, Y.; Kyakuno, H.; Miyata, Y.; Yamamoto, T.; Saito, T.; Hata, K.; Maniwa, Y. Thermoelectric properties of single-wall carbon nanotube films: Effects of diameter and wet environment. *Appl. Phys. Express* **2016**, *9* (2), 025102.
(42) Jo, I.; Kim, Y.; Moon, J.; Park, S.; Moon, J. S.; Park, W. B.; Lee, J. S.; Hong, B. H. Stable n-type doping of graphene via high-molecular-weight ethylene amines. *Phys. Chem. Chem. Phys.* **2015**, *17* (44), 29492−29495.
(43) Sun, B.; Hong, W.; Thibau, E. S.; Aziz, H.; Lu, Z. H.; Li, Y. N. Polyethylenimine (PEI) As an Effective Dopant To Conveniently Convert Ambipolar and p-Type Polymers into Unipolar n-Type Polymers. *ACS Appl. Mater. Interfaces* **2015**, *7* (33), 18662−18671.
(44) Maultzsch, J.; Reich, S.; Thomsen, C.; Webster, S.; Czerw, R.; Carroll, D. L.; Vieira, S. M. C.; Birkett, P. R.; Rego, C. A. Raman characterization of boron-doped multiwalled carbon nanotubes. *Appl. Phys. Lett.* **2002**, *81* (14), 2647−2649.
(45) An, C. J.; Kang, Y. H.; Lee, A. Y.; Jang, K. S.; Jeong, Y.; Cho, S. Y. Foldable Thermoelectric Materials: Improvement of the Thermoelectric Performance of Directly Spun CNT Webs by Individual Control of Electrical and Thermal Conductivity. *ACS Appl. Mater. Interfaces* **2016**, *8* (34), 22142−22150.

https://doi.org/10.1021/jacsau.2c00189
JACS Au 2022, 2, 2269−2276